Magnetic Resonance Imaging 87 (2022) 56–66

Contents lists available at ScienceDirect

Magnetic Resonance Imaging

journal homepage: www.elsevier.com/locate/mri

Accelerated reconstruction of dictionary-based T_2 relaxation maps based on dictionary compression and gradient descent search algorithms

Guy Shpringer [a], David Bendahan [b], Noam Ben-Eliezer [a,c,d,*]

[a] Department of Biomedical Engineering, Tel Aviv University, Tel Aviv, Israel
[b] Aix Marseille University, CNRS UMR 7339, CRMBM, Marseille, France
[c] Sagol School of Neuroscience, Tel Aviv University, Tel Aviv, Israel
[d] Center for Advanced Imaging Innovation and Research (CAI2R), New York University Langone Medical Center, New York, NY, USA

ARTICLE INFO

Keywords:
Magnetic resonance imaging
Principal component analysis
T_2 mapping
Dictionary compression
Gradient descent

ABSTRACT

Background

Quantitative T_2-relaxation-based contrast maps have shown to be highly beneficial for clinical diagnosis and follow-up. The generation of quantitative maps, however, is impaired by long acquisition times, and time-consuming post-processing schemes. The EMC platform is a dictionary-based technique, which involves simulating theoretical signal curves for different physical and experimental values, followed by matching the experimentally acquired signals to the set simulated ones.

Purpose

Although the EMC technique has shown to produce accurate T_2 maps, it involves computationally intensive post-processing procedures. In this work we present an approach for accelerating the reconstruction of T_2 relaxation maps.

Methods

This work presents two alternative post-processing approaches for accelerating the reconstruction of EMC-based T_2 relaxation maps. These are (a) Dictionary compression using principal component analysis (PCA) and (b) gradient-descent search algorithm. Additional acceleration was achieved by finding the optimal MATLAB C++ compiler. The utility of the two suggested approaches was examined by calculating the relative error, produced by each technique.

Results

Gradient descent method was in perfect agreement with the ground truth exhaustive search matching process. PCA based acceleration produced root mean square error (RMSE) of up to 4% compared to exhaustive matching process. Overall acceleration of x16 was achieved using gradient descent in addition to x7 acceleration by choosing the optimal MATLAB C++ compiler.

Conclusions

Postprocessing of EMC-based T_2 relaxation maps can be accelerated without impairing the accuracy of the ensuing T_2 values.

1. Introduction

MRI's transverse (T_2) relaxation time is one of the most commonly used contrast mechanisms for diagnosis and prognosis of pathologies. This relaxation mechanism is most-commonly utilized in a qualitative manner, involving visual assessment of contrast-weighted images. Quantitative mapping of T_2 relaxation times has also shown to be useful for the diagnosis of pathologies including neurodegenerative diseases [1–3] cancer [4–6], impaired hip and knee cartilage [7–12], imaging of stroke [13], assessment of diseased and post-transplant myocardial edema [14,15], and investigation of muscle physiology [16]. Quantitative T_2 mapping (qT_2) offers several advantages. First, it provides the flexibility to generate any level of T_2 contrast offline [17,18]. Second, qT_2 offer higher sensitivity to subtle tissue changes, allowing to detect pathology in an otherwise normal-appearing tissues [3,19,20]. Third, and no less important, is the scalability of the measured values, which are stable across scanners and scan settings, and thus allow easier

* Corresponding author at: Department of Biomedical Engineering, Tel Aviv University, Tel Aviv, Israel.
E-mail address: noambe@tauex.tau.ac.il (N. Ben-Eliezer).

https://doi.org/10.1016/j.mri.2021.12.006
Received 18 June 2021; Received in revised form 19 November 2021; Accepted 22 December 2021
Available online 30 December 2021

Nomenclature

MESE	multi-echo-spin-echo
SE	spin-echo
EMC	echo-modulation-curve
qT_2	quantitative T_2
ETL	echo train length
ROI	region of interest
PD	proton density

longitudinal and multi-center studies [21].

Notwithstanding the proven utility of qT_2, this technique is still underutilized due to the difficulties of reliably quantifying this relaxation time. These include the extensive scan times associated with single spin-echo (SSE) acquisitions [20–24] (ca. 1-h scan for clinically relevant spatial-resolutions), and the contamination of rapid multi-echo spin-echo (MESE) protocols by stimulated echoes (STEs) [21,25–27]. These lead to significant overestimation of T_2 values when using a theoretical exponential fitting [25,28], a bias which is moreover not constant as it depends on the scanner and scan parameters being used [20,21,25,28].

Several approaches have been developed for accurate mapping of T_2 values at clinically-relevant scan times. One class of techniques relies on steady state free precession protocols such as inversion recovery True-FISP [29] and DESPOT2 [30], to avoid contamination of MESE signals by STEs. These protocols are characterized by relatively short scan times on expense of higher sensitivity to main field (B_0) inhomogeneities and reduced T_2 encoding quality vs. spin-echo based protocols [25,29,31–33]. The Extended Phase Graph (EPG) algorithm is another useful technique, developed specifically for modeling MESE STEs by tracking all the coherence pathways along the MESE echo train, while also accounting for imperfect slice profiles [22,30,34–36]. Recently, extensive research has been done regarding the use of dictionary-based signal processing techniques such as magnetic resonance fingerprinting (MRF) [37], and the echo modulation curve (EMC) algorithm [25]. Previous reports have shown the superiority of Bloch-equation based fitting for mapping T_2 values [22], as well as the accuracy and reproducibility of the EMC technique across different scan settings [19,32–34,38]. This advantage can be attributed to the fact that methods like the EMC algorithm incorporate the specific protocol implementation and experimental parameter values into its reconstruction process [3]. Notwithstanding their short scan times, these dictionary-based techniques involve intensive data post-processing procedures, as they require matching the experimental signal from each voxel to each dictionary element, in order to find the best fit between theoretical and experimental data. These exhaustive search procedures are often too time-consuming for realtime processing, thereby hindering the integration of such techniques in clinical settings.

Several techniques have been proposed for accelerating the reconstruction of MRF-based parameter mapping. These may be divided to two classes. The first altogether avoids the use dictionaries by relying on iterative data-driven parameter estimation (Kalman's filter [39]), on nonlinear regression models [40], or based on machine/deep-learning approaches [41–45]. These offer a twofold advantage of skipping the dictionary creation and fitting process – both of which involve computationally intensive procedures. The second class is based on accelerating the dictionary matching process, either through dimensionality reduction of MRF data using singular value decomposition (SVD) [46], low-rank approximation [47], and compressed sensing [48,49]; using fast group matching procedures [50]; or using strong GPU-based computational power [51].

In this work we investigate two approaches for accelerating dictionary-based reconstruction of MESE data. The first approach is to reduce the dimensionality of the search space using dictionary compression based on principal component analysis (PCA) [52,53]; and the second approach improves the efficiency of the dictionary-matching procedure using a gradient descent (GD) search scheme. Improvement in reconstruction times are presented for each approach, demonstrated on in vivo brain and calf data.

2. Material and methods

2.1. MRI scans

MRI scans were performed on a whole-body 3 Tesla MRI scanner (Prisma, Siemens Healthineers). Brain and calf scans of two healthy volunteers were performed under the approval of the ethics committee at Sheba Medical Center, Ramat Gan, Israel. Calf muscles of a genetically-confirmed dysferlinopathy patient were scanned at the Center for Magnetic Resonance in Biology and Medicine, Marseille, France. The patients' protocol was approved by the local ethics committee (Comité de Protection des Personnes Sud Méditerranée I).

Experimental quantitative T_2 data were acquired using a multi-echo spin-echo (MESE) protocol. Brain scans used a 24-channel receiver coil, and the following experimental parameters: TR/TE = 4072/15 ms, slice thickness = 3 mm, number of slices = 26, acquisition bandwidth = 200 Hz/Px, N_{Echoes} = 10, field-of-view = 220 × 206 mm^2, matrix size = 128 × 120. Healthy subjects' calf scans used a flexible 4-channel receive coil and 4 additional coils embedded in the scanner bed, with the following experimental parameters: TR/TE = 3000/10 ms, slice thickness = 4 mm, number of slices = 5, acquisition bandwidth = 200 Hz/Px, N_{Echoes} = 25, field-of-view = 120 × 180 mm^2, matrix size = 106 × 160. Patients' calf scan was performed on a 1.5 Tesla whole-body MR scanner (Siemens Healthineers), using the following experimental parameters: TR/TE = 2500/8.7 ms, slice thickness = 10 mm, number of slices = 5, acquisition bandwidth = 434 Hz/Px, N_{Echoes} = 17, field-of-view = 192 × 192 mm^2, matrix size = 128 × 128.

2.2. Data pre-processing: generation of the EMC dictionary

Quantitative T_2 maps were generated using the EMC algorithm described in [25] and summarized in Appendix A. All procedures were programmed in-house using MATLAB (The MathWorks Inc., Natick, MA), and C++ code compiled to a MATLAB MEX file using the MinGW64 compiler. The EMC algorithm consists of an initial pre-processing stage, in which Bloch simulations of the prospective MESE protocol are performed using the exact RF pulse shapes and other experimental parameter-values used on the MRI scanner. This allows to simulate the actual MESE T_2 decay curve and produce T_2 values that are invariant to the particular choice of scanner and scan settings. Simulations are repeated for a range of T_2 relaxation values and transmit-field (B_1^+) inhomogeneity levels (T_2 = 1…1000 ms, B_1^+ = 70…130%), producing dictionary of echo modulation curves (i.e., EMC's), each associated with a unique [T_2,B_1^+] pair.

2.3. Data post-processing: generation of quantitative T_2 relaxation maps

Once experimental data is acquired, the signal time-series at each voxel is matched to the dictionary of simulated EMCs, by minimizing the l_2-norm of the difference between experimental and simulated curves $\|EMC_{exp} - EMC_{sim}\|_2$. Once a match is found, a unique T_2 value associated with the matched EMC is assigned to the corresponding voxel. Repeating this process for all voxels, yields the desired parametric map. Next, proton density (PD) maps are calculated by extrapolating the image from the first echo time to time $t = 0$, based on the calculated T_2 map, under the assumption that purely exponential decay takes place between excitation and the first TE. This assumption is based on the fact that stimulated echoed affect MESE signals only from the second echo and on, while the first echo includes only spins that underwent perfect refocusing.

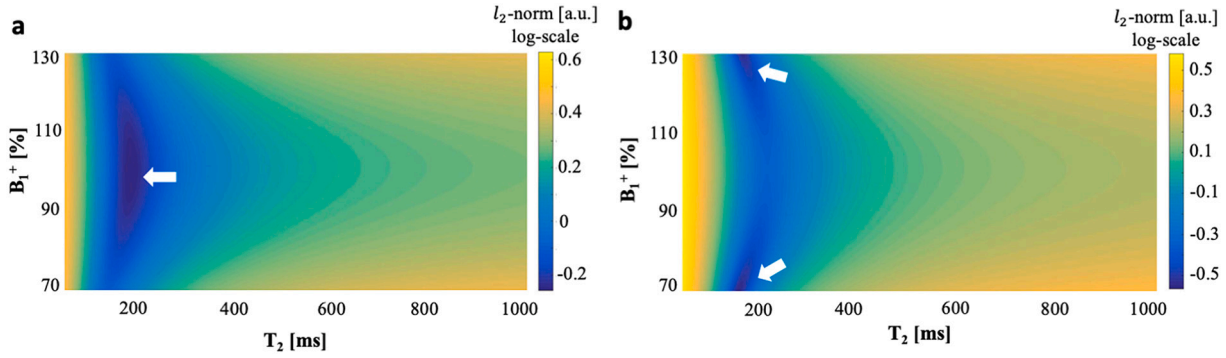

Fig. 1. Graphical representation of the l_2-norm space of a single voxel with respect to the EMC fitting dictionary. Two-dimensional surf plots show the l_2-norm values over the dictionary of EMCs for two representative voxels. (a) l_2-norm space for a voxel where B_1^+ is homogenous resulting in a single minimum point. (b) l_2-norm space for a voxel where B_1^+ is inhomogeneous (e.g. $B_1^+ \pm \Delta B_1^+$), leading to two local minima, and only one global minimum point.

The above fitting process can be implemented using an exhaustive search over the set of $N_{T_2} \times N_{B_1^+}$ dictionary entries (~10,000…20,000 elements). Calculation of the l_2-norm of each element also depends on the MESE echo train length (ETL), which eventually leads to extensive reconstruction times. To overcome this limitation, we investigated two different acceleration approaches: PCA compression of the EMC dictionary and experimental data, and optimized traversal of the dictionary search space using a GD search scheme.

2.4. Accelerated reconstruction using PCA compression

SVD is a mathematical factorization method for real or complex matrices. Every matrix $A \in C^{n\times m}$ can be written using the SVD as:

$$A = U\Sigma V^* \tag{1}$$

where $U \in C^{n\times n}$ and $V \in C^{m\times m}$ are real or complex unitary matrices, and $\Sigma \in R^{n\times m}$ is a diagonal matrix with nonincreasing and nonnegative real numbers, which are the singular values $\sigma_1, \ldots, \sigma_{min(n,m)}$ of the matrix A. The columns of U are denoted as $u_1, \ldots, u_n$ and the columns of V are denoted by $v_1, \ldots v_m$.

One of the common applications of SVD, is to approximate A using a matrix $A^{(r)}$ with lower dimensions. An r-rank approximation of A, where $r \leq min\,(n,m)$, is produced by truncating U and V, and using only the first r columns of U and r rows of V^*, corresponding to the r largest singular values. This can be written as

$$A^{(r)} = \sum_{i=1}^{r} \sigma_i u_i v_i^* \tag{2}$$

The energy of a matrix A is then defined by

$$E = \sum_{i=1}^{min(m,n)} \sigma_i^2 \tag{3}$$

and the *energy ratio* represents the energy conserved in the r-truncation of the matrix, defined by

$$E(r) = \frac{1}{E}\sum_{i=1}^{r} \sigma_i^2 \tag{4}$$

The energy ratio is an important criterion for choosing the truncation rank r, so as to retain most of the energy from the original matrix A. The implementation of PCA as part of a reconstruction procedure is similar to the pattern recognition problem of facial recognition using SVD [54]. In the context of this work, we apply SVD to the dictionary D of simulated EMCs

$$D = U\Sigma V^* \tag{5}$$

where $U \in R^{(N_{T2}\times N_{B1+})\times(N_{T2}\times N_{B1+})}$, $V \in R^{N_{ETL}\times N_{ETL}}$, Σ is as described before, and $D \in R^{(N_{T2}\times N_{B1+})\times N_{ETL}}$ is a dictionary with rank d. The truncated dictionary can then be written as

$$D \approx D^{(r)} = U_r \Sigma_r V_r^* \tag{6}$$

with $r \leq d$. An important property of the SVD is that the right singular vectors form an orthonormal basis for the rows of D. Thus, each entry from the original dictionary can be written as linear superposition of these orthonormal vectors, allowing to express the dictionary in a lower-dimensional space C^r according to

$$D^{(r)} = DV_r \tag{7}$$

The same compression can be applied to the experimental signals using the truncated V_r matrix,

$$EMC_{exp}^{(r)} = EMC_{exp} V_r \tag{8}$$

This being done, the exhaustive procedure of matching experimental and theoretical curves can be done using the compressed dictionary and data. Total computation time includes, in this case, the time required for data compression and for the matching process. The PCA process itself requires $r \times ETL \times N_{voxels}$ operations, while number of computations required for T_2 matching process is $N_{T_2} \times N_{B_1^+} \times r \times N_{voxels}$ vis-à-vis the original matching process which costs $N_{T_2} \times N_{B_1^+} \times N_{ETL} \times N_{voxels}$. The number of computations is thus reduced by a factor of $\sim \frac{ETL}{r}$.

2.5. Accelerated reconstruction using gradient descent (GD) search scheme

GD is a first-order optimization algorithm for finding local minimum of a differentiable function. This technique minimizes an objective function $F(x)$, parameterized using $x \in \mathbb{R}^d$, by updating the parameters in the negative gradient direction of F using $\nabla_x F(x)$. Optimization then follows

$$x_{n+1} = x_n - \eta \nabla_x F(x) \tag{9}$$

where $\eta \in \mathbb{R}^+$ is the step size, and for η small enough we have a decreasing monotonic set $F(x_0) \geq F(x_1) \geq F(x_2) \geq \ldots$. Unlike the continuous case described above, the EMC dictionary involves discrete T_2 and B_1^+ values. A discrete search problem can be formulated, in this case, using graph theory where the set of vertices S denote locations in dictionary space:

$$S = \left\{ (T_2, B_1^+) \mid T_2 \in [T_{2_{min}}, T_{2_{max}}] \; and \; B_1^+ \in \left[B_{1_{min}}^+, B_{1_{max}}^+\right] \right\} \tag{10}$$

and the set of edges $E \subseteq S \times S$ denote the connection between each pair of vertices. The problem of finding a unique pair $[T_2, B_1^+]$ with the minimal l_2-norm $\|EMC_{exp} - EMC_{sim}\|_2$, now translates to searching through a *weighted* graph, where the weight between edges is defined as:

$$w(S_1, S_2) = \left\|EMC_{exp} - EMC_{sim,S_1}\right\|_2 - \left\|EMC_{exp} - EMC_{sim,S_2}\right\|_2 \tag{11}$$

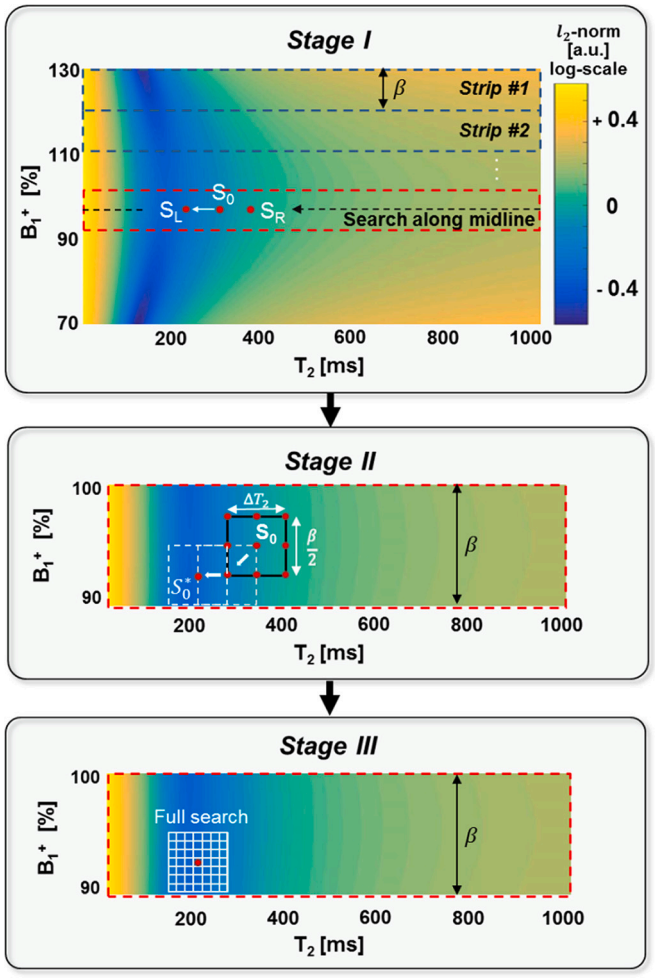

Fig. 2. Gradient-descent search algorithm. The algorithm implements fast traversal over the l_2-norm space of every voxel in order to find the minimal [T_2, B_1^+] value pair. *Stage I:* the l_2-norm space is divided to strips, where β represent number of B_1^+ values in each strip. A three-vertices search scheme (S_L, S_0, S_R) is performed, until the mid-point S_0 assumes the minimal value. *Stage II:* A nine-vertices search scheme is performed (nine red dots in the Figure). In each iteration the center vertex of the search window (solid black rectangle) is shifted to the minimum valued vertex (S_0*) until the center vertex assumes the minimal value out of the nine vertices. *Stage III:* A full exhaustive search is performed across all vertices in the search window, centered around S_0*. (For interpretation of the references to colour in this figure legend, the reader is referred to the web version of this article.)

where EMC_{exp} is the experimental EMC being analyzed, and $EMC_{sim,\ S_1}$ and $EMC_{sim,\ S_2}$ denote the simulated EMCs for values of [T_2,B_1^+] assigned to vertex S_1 and S_2, respectively. Using these definitions, it is possible to implement a discrete GD procedure, with the gradient between two vertices defined as the weight of the edge connecting them.

The l_2-norm difference between the experimental EMC of an arbitrary voxel and the dictionary of simulated EMCs can be graphically represented as a function of T_2 and B_1^+ as shown in Fig. 1. This graphical representation highlights two important properties of the l_2-norm search space: first, it is monotonic in the neighborhood of each local minima, and second, it can have either one or two minima. A voxel residing in a region where B_1^+ is homogeneous would have a single minimum point, while regions of inhomogeneous B_1^+ fields will result in two minima due to the symmetry of B_1^+ around its undistorted value (see supplementary Fig. S.1). GD search through this space is done in three stages. *Stage I*: the l_2-norm space is divided into horizontal strips along the B_1^+ dimension, i.e. each strip consists all the simulated T_2 values and a limited range of $\beta = 10$ B_1^+ values, resulting in $N_{B_1^+}/\beta$ strips (see Fig. 2 Stage I). The local minimum within each strip is found by sampling the T_2 dimension using a three-vertices search scheme. These are defined as:

$$S_0 = \left[T_2^0, B_1^{+0}\right]$$

$$S_L = \left[T_2^0 - \frac{\Delta T_2}{2}, B_1^{+0}\right] \tag{12}$$

$$S_R = \left[T_2^0 + \frac{\Delta T_2}{2}, B_1^{+0}\right]$$

Here $\Delta T_2 = 20$ ms is the configurable width of the search window, the initial B_1^{+0} is set to be the middle of the strip, the initial T_2^0 is set to 100 ms, and $S_{L/R}$ are the left/right edges of the search window. The use of $\Delta T_2 \gg 1$ allows fast traversal through the strip, thereby accelerating the search procedure. As long $w(S_0, S_L) \leq 0$ or $w(S_0, S_R) \leq 0$, another iteration is done and the center vertex S_0 is updated to be S_L or S_R, respectively. The stopping criterion is when both weights of the edges are positive.

Stage II: once the region of the minimal value is found, a 9-vertices search scheme is applied on a rectangular window centered at the output vertex of previous scheme. The window has a width ΔT_2 along the T_2 dimension and height $\beta/2$ along the B_1^+ dimension. The 8 other vertices are the corners of the search window mid-points at each side (see Fig. 2 Stage II). Same GD scheme is then applied to shift the window center to the vertex with the largest gradient from the center vertex. This continues until all the edges (the gradients) have positive values, i.e. the center vertex has the minimal value amongst all the 9 vertices. At *Stage III*, an.

exhaustive search is performed within the $\Delta T_2 \times (\beta/2)$ rectangular search window, i.e. iterating across all dictionary entries within this window and calculating their l_2-norm value to find the minimal one. Once a minimal value is found for each strip, the global l_2-norm minimum value is obtained as the minimal value across all strips, producing the voxels [T_2,B_1^+] value pair. Repeating this process for each voxel produces full T_2 and B_1^+ maps.

Once these three stages are performed, the calculated B_1^+ map is re-processed to remove outliers and perform spatial smoothing in order to reflect a realistic continuous transmit profile (see Appendix A). The resulting map B_1^+ is inputted into a second matching process, which is similar to the first one, albeit having only a limited range of B_1^+ values per voxel, equal to the input values ± 3%. The second iteration is thus done on only one strip, around the inputted B_1^+ from the first iteration.

2.6. Estimation of relative error when using accelerated reconstruction

The accuracy of each accelerated reconstruction technique was estimated vis-à-vis full exhaustive search of the entire dictionary space. The relative percent error was then estimated at each voxel and for each reconstruction technique. Mean and standard deviation were then calculated across all voxels in the slice. To focus the error estimation on the physiologically relevant T_2 range we excluded T_2 values larger than 200 ms and smaller than one TE (typically 10 ms). The two assayed anatomies were reconstructed using dictionaries having the same number of entries. This was done in order to factor out the effect of the number of entries on the reconstruction time, and the resulting acceleration factors.

2.7. C/C++ MATLAB compiler considerations

All computations were performed using MATLAB on a standard desktop computer. Part of the reconstruction is implemented in C++ function, which is compiled using one of MATLAB's recommended compilers, and invoked using MATLAB's MEX interface. In this work the performances of two compilers, the default Microsoft Visual Studio Compiler (MSVC) and minGW-64, were tested for variation in

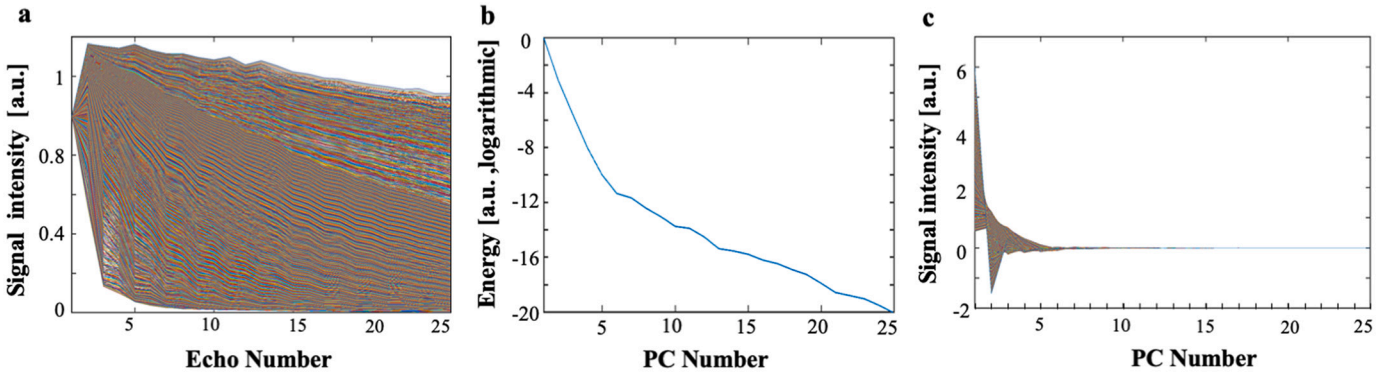

Fig. 3. PCA based compression of an EMC dictionary. Dictionary compression was done by calculating the energy of each principal component in the SVD, in order to evaluate the number of principal components that contain meaningful information and are needed for image reconstruction. (a) Original EMC dictionary. (b) Relative energy of each principal component [logarithmic scale]. (c) EMC dictionary, spanned in PCA space, attesting to the low rankness of the dictionary matrix and its compressibility.

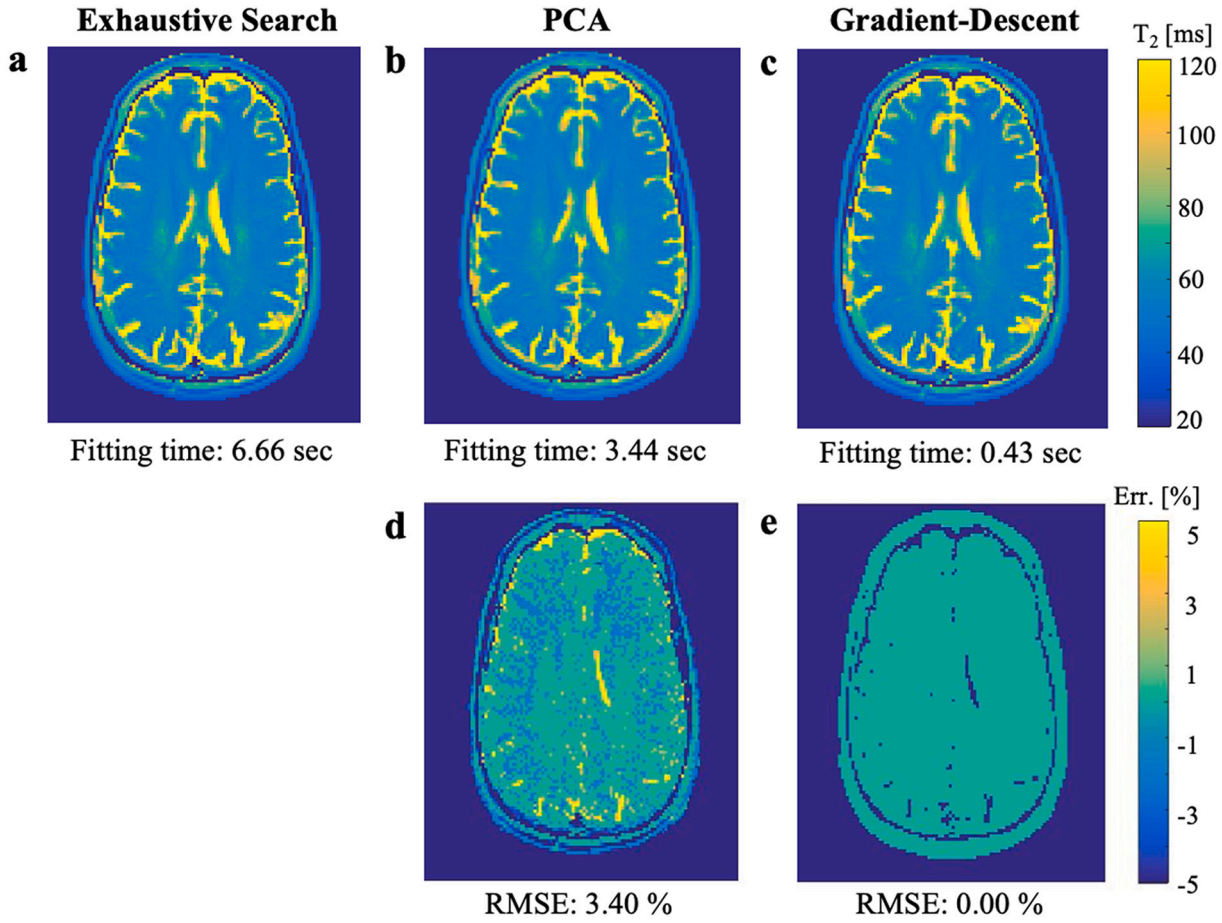

Fig. 4. Accelerated reconstruction of T_2 maps of the brain. Quantitative T_2 maps and relative-error maps, using PCA and GD accelerated reconstruction schemes. (a) T_2 map reconstructed using exhaustive search method, with fitting time of 6.66 s per slice [matrix size = 120 × 128]. (b-c) T_2 maps that were fitted using the PCA and GD techniques, with fitting times of 3.44 and 0.43 s per slice respectively. (d-e) Relative-error of the PCA and GD accelerated reconstruction schemes produced RMSE of 3.40% and 0.00% respectively.

computation speed.

3. Results

Comparing the postprocessing times of several datasets we found that the minGW-64 compiler provided superior performance, leading to a significant x7 decrease in reconstruction times compared to the MSVC compiler. The results presented hereon are thus shown for the minGW-64 compiled MEX libraries.

3.1. Accelerated reconstruction of T_2 maps using SVD dictionary compression

Fig. 3 shows the feasibility of compressing an EMC dictionary using

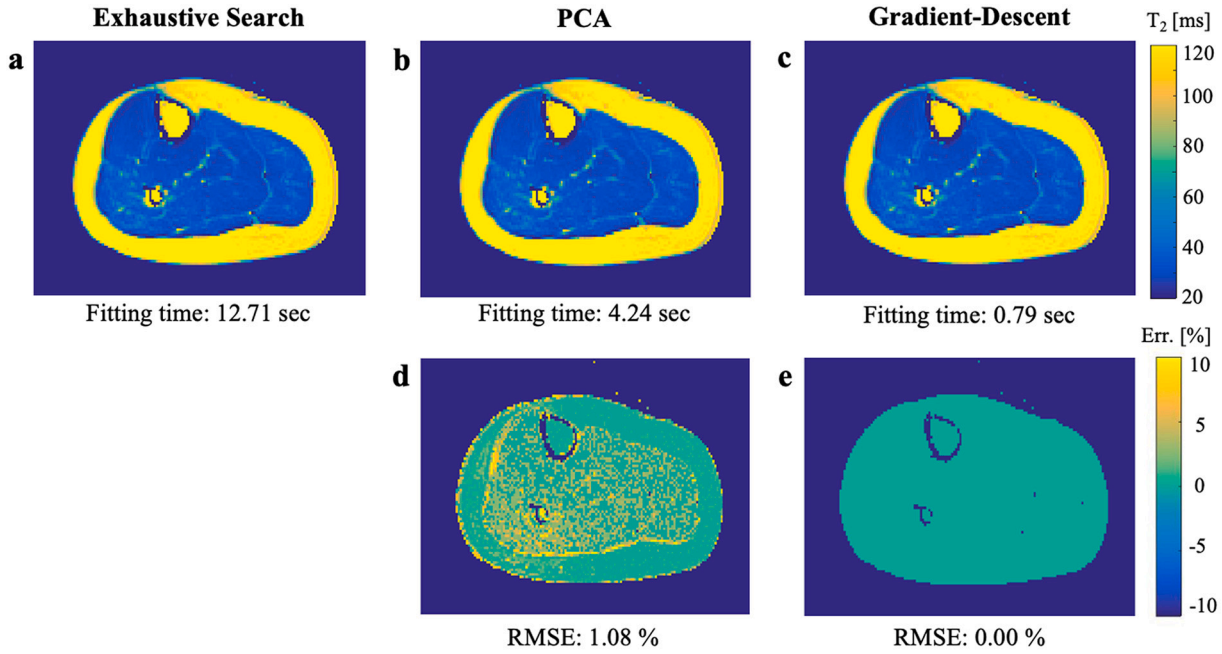

Fig. 5. Accelerated reconstruction of T_2 maps of the calf. Quantitative T_2 maps and relative-error maps, using PCA and GD accelerated reconstruction schemes. (a) T_2 map reconstructed using exhaustive search method, with fitting time of 12.71 s per slice [matrix size = 106 × 160]. (b-c) T_2 maps that were fitted using the PCA and GD techniques, with fitting times of 4.24 and 0.79 s per slice respectively. (d-e) Relative-error of the PCA and GD accelerated reconstruction schemes produced RMSE of 1.08% and 0.00% respectively.

PCA. A graph of the relative energy of each PC is shown in Fig. 3b for a representative dictionary. The PC values are sorted in logarithmic nonincreasing order, exhibiting a fast drop in each PC's energy and a change in slope of the graph beginning at approximately the 5th PC. Fig. 3a and c show the original and compressed dictionaries after the PCA projection. Consistent with the slope in Fig. 3b, most of the signal in the PCA projected dictionary is concentrated in the first 5–6 PCs, suggesting that it is possible to project the dictionary (and the experimental EMC data) onto the first five eigenvectors in order to accelerate the dictionary search process.

Figs. 4b and 5b show quantitative T_2 maps produced using PCA-based accelerated reconstruction of brain and calf anatomies of healthy subjects. A full exhaustive search produces the ground truth maps are shown in Figs. 4a and 5a, with the voxel-wise error maps shown in Figs. 4d and 5d respectively. Error values represent absolute relative error with respect to the full exhaustive search, producing mean RMSE of 3.4% for the brain anatomy, and mean RMSE of 1.1% for the calf anatomy, using the PCA acceleration. Total fitting time for the brain anatomy using the PCA scheme is 89.44 s (for 26 slices), reflecting a reduction of 48.3% with respect to the fitting time using exhaustive search. For the calf anatomy the total fitting time is 21.2 s (for 5 slices), reflecting a 66.6% decrease with respect to the exhaustive search scheme.

3.2. *Accelerated reconstruction of T_2 maps using gradient descent method*

The second approach for accelerating the EMC fitting process was based on an efficient search pattern in the dictionary search-space. Fig. 1 shows two typical l_2-norm spaces for two representative voxels. Figs. 4c, e and 5c,e show quantitative T_2 maps reconstructed using GD search pattern along with the corresponding fitting errors for healthy brain and calf anatomies scans. The GD scheme produced 100% accuracy in the T_2 calculated values. Total fitting time for the brain anatomy (26 slices) using the GD scheme is 11.18 s, reflecting a reduction of 93.5% in the overall fitting time compared to the exhaustive search scheme. For the calf anatomy (5 slices), the total fitting time is 3.95 s, reflecting a reduction of 93.8% in the overall fitting time compared to the exhaustive search scheme. Fig. 6 shows a quantitative T_2 map for a patient with

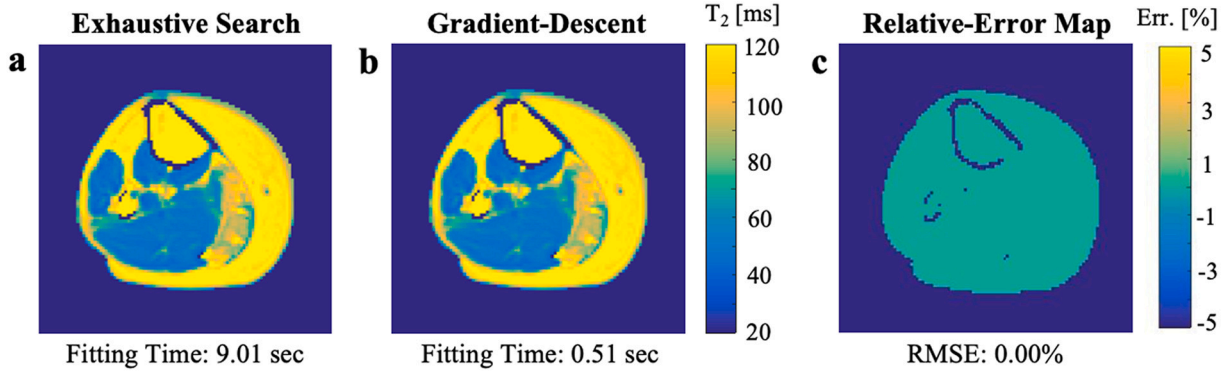

Fig. 6. Accelerated reconstruction of T_2 maps of a dysferlinopathy patient's calf anatomy. (a) T_2 map reconstructed using exhaustive search, with fitting time of 9.0 s per slice [matrix size = 128 × 128]. (b-c) Gradient descent fitting of the same anatomy took 0.5 s per slice, with zero RMSE.

Table 1
Performance and accuracy of the accelerated PCA and gradient descent (GD) fitting techniques for brain and calf anatomies.

Fitting method↓	Anatomy [# slices]→	Brain [26]	Calf #1 [5]	Calf #2 [5]
	No. of voxels →	366,782	78,758	67,939
	Matrix size →	120 × 128	106 × 160	128 × 128
Exhaustive search [ground truth]	Total duration [*sec*]	173.2	63.6	45.3
	Duration per slice [sec]	6.66	12.71	9.01
	Duration per voxel [ms]	0.47	0.81	0.67
PCA	Total duration [sec]	89.4	21.2	20.9
	Duration per slice [sec]	3.44	4.24	4.19
	Duration per voxel [ms]	0.24	0.27	0.30
	Acceleration Factor	1.9	3.0	2.2
	Relative error [%]	3.4 ± 1.6	3.0 ± 5.4	4.5 ± 6.0
Gradient descent	Total duration [sec]	11.1	3.9	2.6
	Duration per slice [sec]	0.43	0.79	0.51
	Duration per voxel [ms]	0.03	0.05	0.04
	Acceleration Factor	15.5	16.1	17.5
	Relative error [%]	0.0 ± 0.0	0.0 ± 0.04	0.0 ± 0.0

The exhaustive search approach produced ground truth maps which were compared against the two accelerated techniques. Measured parameters include the mean and standard deviation of the relative error across all voxels within the examined anatomy. Voxels with T_2 values larger than 200 ms, and shorter than 10 ms were excluded as they correspond to tissues with lower clinical relevance (excluding CSF, which requires an entirely different range of experimental TEs in order to be estimated). As can be seen, the GD technique achieved perfect reconstruction, with acceleration factors of 15–18 for a dictionary comprised of 203 T_2 × 41 B_1^+ entries.

dysferlinopathy. Fig. 6a shows the original T_2 map reconstructed using the exhaustive search process, while Fig. 6b shows the T_2 map reconstructed using the accelerated GD scheme. Similar to the healthy subjects' results, no error was produced when employing the GD reconstruction scheme, which offered 94.3% reduction in the map's fitting time.

3.3. Evaluating reconstruction properties

Table 1 summarizes the acceleration factors and corresponding relative errors achieved for each anatomy. GD-based method produced almost perfect reconstruction, with improved acceleration factors compared to the PCA dictionary compression approach. Reconstruction times were calculated for both multi-slice scans and also per single/voxel. These acceleration factors depended mainly on the dictionary size, namely, the number of simulated T_2 and B_1^+ values, as well as on the number of acquired echoes (experimental ETL). The ETL defines, in this case, the number of core operations involved in matching the experimental signal in a single voxel to a single dictionary element. Thus, shorter ETLs resulted in higher relative acceleration factors, although the absolute change in processing time remained the same. The performance of the GD acceleration technique depended on the l_2-norm space of the fitted voxel (which depends mainly on B_1^+ uniformity), and on the different range of T_2 values in each anatomy, affecting the number of echoes used in the calculation of the l_2-norm between experimental and simulated EMCs.

4. Discussion

In this study we investigated two approaches for accelerated fitting of dictionary-based T_2 mapping from MESE data. The original and straightforward fitting procedure involved an exhaustive search over an entire dictionary space, which is time consuming and limits the clinical applicability of EMC-based T_2 mapping. Our results show that the GD search pattern affords significant reduction in the processing time and that choosing the right C++ compiler also has a dramatic effect, which can reduce the overall reconstruction times by an additional x7 factor.

The PCA-based dictionary compression approach resulted in non-negligible inaccuracies in the fitted T_2 values. These inaccuracies may be a result of two inherent issues of the PCA algorithm. First, the compression process involves reducing the dimensionality of the dictionary using an SVD approximation process and removing PCs below a certain threshold. This involves an unavoidable loss of information, creating a trade-off between the accuracy of the reconstruction process and the number of principal components retained in the compressed dictionary. Secondly, the l_2-norm search spaces are different for different T_2 baselines, leading to T_2 dependent errors in the PCA fitting process.

A few important insights can be drawn regarding the search process by examining the l_2-norm space of fitted voxels. First observation is that an ambiguity arises in this search space at areas of inhomogeneous B_1^+, resulting from symmetry of the Bloch equations around the central B_1^+ = 100% value. This ambiguity leads to the emergence of two local minima, which requires to separate the graph to two sub-graphs, and perform a separate search in each one. The final (absolute) minimum [T_2,B_1^+] value pair is then found by comparing the two local minima. The ambiguity of the l_2-norm search-space also highlights the importance of the B_1^+ map smoothing process during the second-stage of the matching process. As the B_1^+ map is expected to be smooth, this constraint helps to overcome cases where one of the two local minima is wrongly identified as the global minimum due to noise. This is particularly important at low SNR settings or when fitting short T_2 components, which are inherently noisy due to their fast signal decay.

Notwithstanding the fitting accuracy, the acceleration factor was very similar across data sets when using dictionaries with similar number of entries. The acceleration factor of the PCA method is a result of using truncated dictionaries. The search process itself is, in this case, the same as in the exhaustive search scheme and therefore depends only on the number of simulated [T_2,B_1^+] pairs and the ratio between ETL and the number of principal components used. The common factors, affecting both acceleration schemes are the matrix-size and number of slices in the scanned dataset – both of which have a linear effect on the acceleration factor as the algorithm iterates over all the pixels in the reconstructed T_2 map and over all slices.

The reconstruction time of the GD search scheme is mainly affected by the number of entries in the simulated dictionary, which can increase the steps that are needed to convergence. Although it is very important property which can be controlled by the resolution of the simulated dictionary, the gradients across the l_2-norm of the map are the most significant property, affecting the reconstruction time. These gradients depend on strength, or level of the T_2 encoding, e.g., using refocusing flip angles smaller than 180° would lead to weaker T_2 weighting, thereby influencing the ability to discern between neighboring T_2 values by decreasing the convexity of the l_2-norm search space, hence the optimal GD step size. The use of l_2-norm is also an important factor as it determines the computational complexity of each step during the matching process (either PCA or GD based). Other criteria for comparing the similarity between experimental and simulated curves can be implemented, e.g., simple correlation, or dot product. These, however, are more suitable for dictionaries in which the entries are orthogonal to one another, in contrast to the low-rank EMC dictionary used here. A small improvement in processing time can be achieved by switching to a simpler similarity criterion, yet, this will not significantly change the

overall runtime process, as each of these criteria involve an O(n) number of operations (where n is the vectors' length).

5. Conclusions

In this paper, we present two approaches for accelerating the reconstruction of quantitative T_2 maps from MESE data using the EMC algorithm. The PCA based compression method is used to reduce the dimensions for both the simulated dictionary and acquired data so as to perform the search over shorter vectors. This approach, however, results in inaccuracies in the calculated T_2 maps, while providing only moderate acceleration factors. The GD-based approach, on the other hand, yielded significant acceleration factors and close to perfect fitting accuracy in comparison to a full exhaustive search. In addition to accelerating the reconstruction process, we have also accelerated the dictionary generation process as can be seen in Appendix B. We believe that these advances will facilitate integration of realtime quantitative T_2 mapping in clinical settings. Future work may be focused on further acceleration using advanced hardware solutions, e.g. using GPUs or artificial intelligence tools.

Acknowledgement

This research was funded by the ISF Israeli Science Foundation Grant 2009/17. The authors have no other conflicts of interest to declare.

Appendix A. The EMC Algorithm

This appendix contains a concise description of the steps for generating T_2 maps using the EMC algorithm, covering the data acquisition, pre-processing, and post-processing procedures.

Step 1 – MRI data acquisition

Experimental data is acquired using a multi-echo spin-echo (MESE) protocol, producing a time-series of T_2 weighted DICOM images, corresponding to increasing echo-times (TEs).

Step 2 – Pre-processing: Generation of a simulated EMC dictionary

Tracking the precise magnetization evolution during a MESE scan is done using simulations of the prospective pulse sequence, programmed in-house in C++ and MATLAB (The MathWorks Inc., Natick, MA) and based on time and space propagation of Bloch equations. The exact pulse sequence scheme and the corresponding parameter values are obtained through offline simulation of the pulse sequence diagram extracted using Siemens's POET sequence testing tool. This provides information regarding the amplitudes and timing of each RF and gradient pulse. The actual RF pulse shapes were read from the pulse sequence source code and imported into MATLAB.

Although full volumetric simulations would have been ideal for EMC modeling, such simulations are not feasible due to their extreme computational intensity, and the extended runtimes that are needed in order to track a pool of $10^3 \ldots 10^4$ spins in a high resolution four-dimensional space (x, y,z,t). To facilitate this process, reduced one-dimensional imaging simulations are carried out solely along the slice dimension (see ref. [6] for justification of this procedure). The internal spatial resolution of these simulations is set high enough to accurately account for intra-voxel dephasing (10–100 μm for data acquired on standard clinical scanners), while the temporal resolution is matched to the one used in the actual MESE experiment.

Each run of the simulation generates a single echo-modulation-curve, designating the intensity of a MESE echo train for a given parameter set. A dictionary of simulated EMCs is thus constructed by repeating the simulations for a range of $T_2 = 1 \ldots 1000$ ms, and transmit field (B_1^+) inhomogeneity scales of 70% and 130%, where a value of 100% corresponds to a purely homogeneous B_1^+ field (see Fig. A.1). The total simulation time depends on the echo train length and number of T_2 and B_1^+ values simulated, with typical times ranging between 1 and 4 h on a multi core desktop PC.

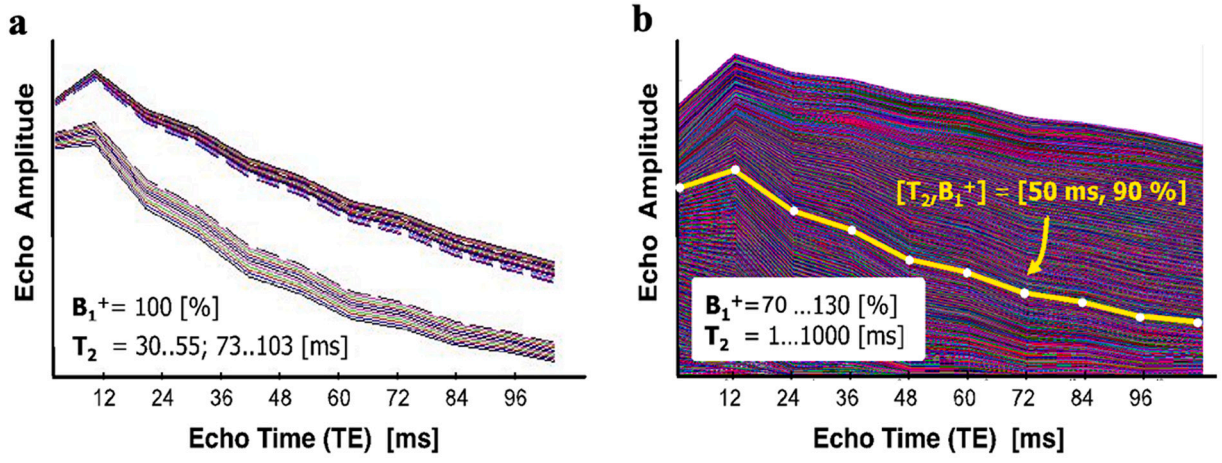

Fig. A.1. Two examples of simulated echo-modulation-curve (EMC) dictionaries for a multi-echo spin-echo (MESE) protocol. (a) A simplified dictionary containing two limited ranges of consecutive T_2 values. (b) Full dictionary, spanning T_2 range of 1…1000 ms and B_1^+ inhomogeneity scales of 70%...130%. The yellow line illustrates an experimentally acquired EMC for a single pixel, which was matched to the dictionary of simulated EMCs producing a specific pair of [T_2, B_1^+] values.

Step 3 – Postprocessing: Generation of T_2, B_1^+ and Proton-Density (PD) maps

Quantitative T_2 values are generated on a pixel-by-pixel basis from the MESE DICOM series by matching the experimental EMC in each pixel to the pre-calculated dictionary of simulated EMCs. Matching is done by calculating the l_2-norm of the difference between the experimental and simulated EMCs, and choosing the EMC yielding the minimal norm value. Following this procedure, a unique pair of [T_2, B_1^+] values is assigned to each pixel, yielding the desired T_2 parametric map of the anatomy. Finally, proton density maps are calculated by extrapolating the intensity of each pixel in the image from the first echo-time (t = TE) to the time point $t = 0$ using the fitted T_2 map according to:

$$PD(x,y) = \frac{S(x,y,t=TE)}{e^{-TE/T_2(x,y)}} \tag{A.1}$$

Appendix B. Accelerating the generation of EMC dictionaries

Generation of EMC dictionaries requires to simulate the propagation of magnetization in a MESE protocol for a range of T_2 and B_1^+ values. Each run of the simulation generates a single EMC. The time required for simulating an entire dictionary will depend on the range of simulated T_2 and B_1^+ values, and on the echo train length. An effective way to accelerate the generation of EMC dictionaries is to decimate the range of simulated T_2 and B_1^+ values and fill in the missing entries by a much faster interpolation procedure. The type of interpolation may vary from simple linear interpolation to more complex techniques. Here, we employed MATLAB's C2 spline interpolation, which was found to produce the most accurate results [55].

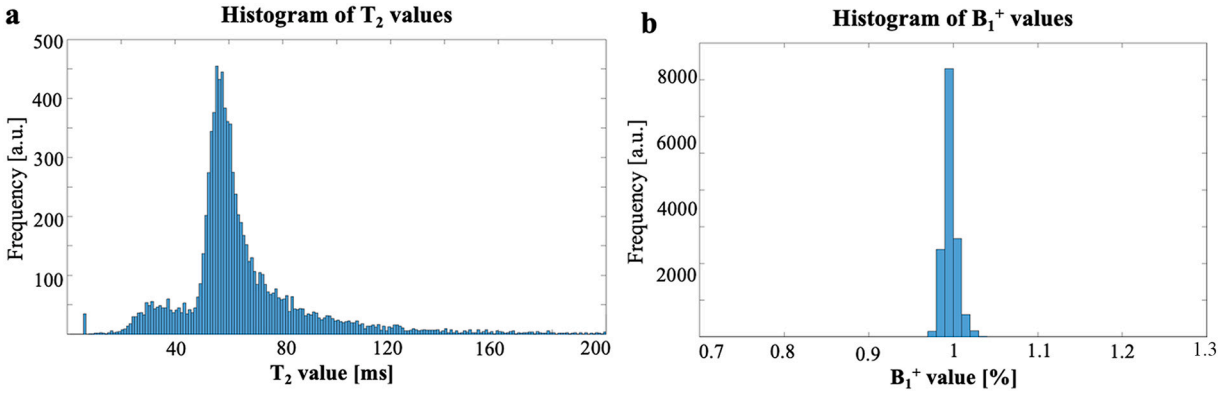

Fig. B.1. Histograms of T_2 and B_1^+ values in a typical brain scan. Values were calculated using the EMC algorithm [56].

To demonstrate the effectiveness of this acceleration technique we consider here a standard dictionary containing 440 T2 values with 1 ms resolution in the range 1…300 ms, and 50 ms resolution in the range 300…1000 ms; and 61 B1+ values in the range 70…130% and resolution of 1%. Before generating a decimated dictionary, we examined the typical T2 and B1+ content of a brain anatomy (shown in Fig. B.1). As can be seen, this anatomy contains a relatively wide range of T2 values but only a limited range of B1+ values, centered around B1 + =100%.

Following this we decimated the original dictionary to contain 21% of the original dictionary's entries, potentially reducing the dictionary generation time by 79%. The ranges of simulated T_2 and B_1^+ values were 1:1:40, 42:2:80, 84:4:160, 200:40:280, 320:80:1000 ms, and 70:2:130% respectively. The mean difference between the interpolated and original dictionaries was 0.0011 % ± 0.0033%. This will depend on the level of decimation, which is recommended to follow a logarithmic scale along the T_2 dimension, starting with small spaced sampling at low T_2 values, and gradually increasing towards larger T_2 values. Fig. B.2a–b presents T_2 maps reconstructed using the fully-simulated and decimated dictionaries. A map of the relative-error of T_2 values that were fitted using the two dictionaries is shown in Fig. B.2c. As can be seen, the two fitting procedures produces almost identical maps, except for a few small errors of <2%, appearing in the CSF region where T_2 values are well beyond the range of TE's that were sampled during the scan (TE = 10:10:20 ms). These results confirm that the generation of EMC dictionaries can be significantly accelerated without loss of clinical information.

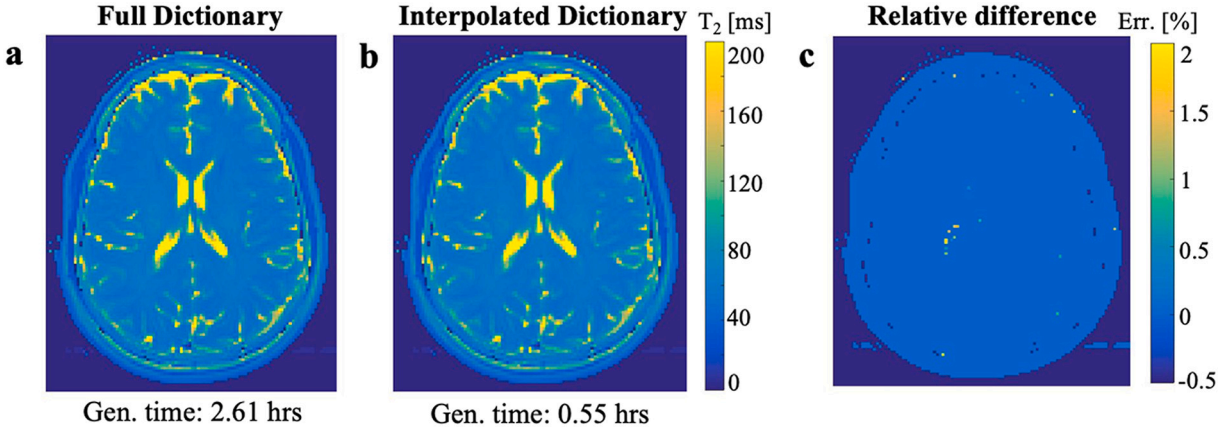

Fig. B.2. Comparison of T_2 maps reconstructed using (a) a fully simulated dictionary vs. (b) a dictionary that was decimated and interpolated. The generation times of the two dictionaries were 2.61 h and 0.55 h respectively. (c) Relative-error between the two maps showing no significant error aside from a few <2% errors inside the CSF.

Appendix A. Supplementary data

Supplementary data to this article can be found online at https://doi.org/10.1016/j.mri.2021.12.006.

References

[1] Ceccarelli A, Rocca MA, Neema M, Martinelli V, Arora A, Tauhid S, et al. Deep gray matter T_2 hypointensity is present in patients with clinically isolated syndromes suggestive of multiple sclerosis. Mult Scler 2010;16:39–44. https://doi.org/10.1177/1352458509350310.

[2] Lund H, Jønsson A, Andresen J, Rostrup E, Paulson OB, Sørensen PS. Cognitive deficits in multiple sclerosis: correlations with T2 changes in normal appearing brain tissue. Acta Neruologica Scand 2012;125:338–44. https://doi.org/10.1111/j.1600-0404.2011.01574.x.

[3] Shepherd TM, Kirov II, Charlson E, Bruno M, Babb J, Sodickson DK, et al. New rapid, accurate T2 quantification detects pathology in normal-appearing brain regions of relapsing-remitting MS patients. NeuroImage Clin 2017;14:363–70. https://doi.org/10.1016/j.nicl.2017.01.029.

[4] Roebuck JR, Haker SJ, Mitsouras D, Rybicki FJ, Tempany CM, Mulkern RV. Carr-Purcell-Meiboom-Gill imaging of prostate cancer: quantitative T_2 values for cancer discrimination. Magn Reson Imaging 2009;27:497–502. https://doi.org/10.1016/j.mri.2008.08.001.

[5] Remmele S, Xu S, Liu W, Turkbey B, Se J, Kruecker J, et al. Accelerated T 2 mapping for characterization of prostate cancer. Magn Reson Med 2011;65:1400–6. https://doi.org/10.1002/mrm.22874.

[6] Farraher SW, Chang KJ, Ozonoff A, Soto JA. Differentiation of hepatocellular carcinoma and hepatic metastasis from cysts and hemangiomas with calculated T_2 relaxation times and the T_1/T_2 relaxation times ratio. J Magn Reson Imaging 2006;24:1333–41. https://doi.org/10.1002/jmri.20758.

[7] Mosher TJ, Dardzinski BJ, Ph D. Cartilage MRI T2 relaxation time mapping: overview and applications. Semin Muscuoloskeletal Radiol 2004;1:355–68.

[8] Pan J, Pialat J-B, Joseph T, Kuo D, Joseph GB, Nevitt MC, et al. Knee cartilage T2 characteristics and evolution in relation to morphologic abnormalities detected at 3-T MR imaging: a longitudinal study of the normal control cohort from the Osteoarthritis Initiative. Radiology 2011;261:507–15.

[9] Nishii T, Shiomi T, Tanaka H, Yamazaki Y, Murase K, Sugano N. Loaded cartilage T2 mapping in patients with hip dysplasia. Radiology 2010;256:955–65.

[10] Son M, Goodman SB, Chen W, Hargreaves BA, Gold GE, Levenston ME. Regional variation in T1ρ and T2 times in osteoarthritic human menisci: correlation with mechanical properties and matrix composition. Osteoarthr Cartil 2013;21:796–805. https://doi.org/10.1016/j.joca.2013.03.002.

[11] Lindner D, Chechik Y, Beer Y, Tal S, Lysyy O, Blumendfeld-Katzir T, et al. T2 mapping values in postmeniscectomy knee articular cartilage after running: early signs of osteoarthritis? J Knee Surg 2020. https://doi.org/10.1055/5-0040-1718596.

[12] Ben-eliezer N, Raya JG, Babb JS, Youm T, Sodickson DK, Lattanzi R. A new method for cartilage evaluation in femoroacetabular impingement using quantitative T2 magnetic resonance imaging: preliminary validation against arthroscopic findings. Cartilage 2019. https://doi.org/10.1177/1947603519870852.

[13] Siemonsen S, Mouridsen K, Holst B, Ries T. Quantitative T_2 values predict time from symptom onset in acute stroke patients. Stroke 2009;40:1612–6. https://doi.org/10.1161/STROKEAHA.108.542548.

[14] Giri S, Chung Y, Merchant A, Mihai G, Rajagopalan S, Raman SV, et al. T_2 quantification for improved detection of myocardial edema. J Cardiovasc Magn Reson 2009;11:1–13. https://doi.org/10.1186/1532-429X-11-56.

[15] Shah S, Giri S, Cotts W, Mcgee E, Gordon R, Collins JD, et al. Cardiac magnetic resonance T_2 mapping in the monitoring and follow-up of acute cardiac transplant rejection a pilot study. Circ Cardiovasc Imaging 2012;5:782–90. https://doi.org/10.1161/CIRCIMAGING.111.971101.

[16] Patten C, Meyer RA, Fleckenstein JL. T_2 mapping of muscle. Semin Muscuoloskeletal Radiol 2003;7:297–307. https://doi.org/10.1055/s-2004-815677.

[17] Sati P, George IC, Shea CD, Gaitán MI, Reich DS. FLAIR*: a combined MR contrast technique for visualizing white matter lesions and parenchymal veins. Radiology 2012;265:926–32.

[18] Fabes J, Matthews L, Filippini N, Talbot K, Jenkinson M, Turner MR. Quantitative FLAIR MRI in amyotrophic lateral sclerosis. Acad Radiol 2017;24:1187–94. https://doi.org/10.1016/j.acra.2017.04.008.

[19] Knight MJ, Mccann B, Tsivos D, Couthard E, Kauppinen RA. Quantitative T_1 and T_2 MRI signal characteristics in the human brain: different patterns of MR contrasts in normal ageing. Magn Reson Mater Physics, Biol Med 2016;29:833–42. https://doi.org/10.1007/s10334-016-0573-0.

[20] Knight MJ, Mccann B, Tsivos D, Dillon S, Coulthard E, Kauppinen RA. Quantitative T2 mapping of white matter: applications for ageing and cognitive decline. Phys Med Biol 2016;61:5587–605. https://doi.org/10.1088/0031-9155/61/15/5587.

[21] Gracien R-M, Maiworm M, Brüche N, Shrestha M, Ulrike N. How stable is quantitative MRI ? – assessment of intra- and inter-scanner-model reproducibility using identical acquisition sequences and data analysis programs. Neuroimage 2020;207:1–11. https://doi.org/10.1016/j.neuroimage.2019.116364.

[22] Mcphee KC, Wilman AH. Transverse relaxation and flip angle mapping: evaluation of simultaneous and independent methods using multiple spin echoes. Magn Reson Med 2017;77:2057–65. https://doi.org/10.1002/mrm.26285.

[23] Hahn EL. Spin echoes. Phys Rev 1950;80:580–94. https://doi.org/10.1103/PhysRev.80.580.

[24] Liney GP, Knowles AJ, Manton DJ, Turnbull LW, Blackband SJ, Horsman A. Comparison of conventional single echo and multi-echo sequences with a fast spin-echo sequence for quantitative T2 mapping: application to the prostate. J Magn Reson Imaging 1996;6:603–7. https://doi.org/10.1002/jmri.1880060408.

[25] Ben-Eliezer N, Sodickson DK, Block KT. Rapid and accurate T_2 mapping from multi-spin-echo data using bloch-simulation-based reconstruction. Magn Reson Med 2015;73:809–17. https://doi.org/10.1002/mrm.25156.

[26] Burstein D. Stimulated echoes: description, applications, practical hints. Concepts Magn Reson 1996;8:269–78. https://doi.org/10.1002/(SICI)1099-0534(1996)8:4<269::AID-CMR3>3.0.CO;2-X.

[27] Constable RT, Anderson AW, Zhong J, Gore JC. Factors influencing contrast in fast spin-echo MR imaging. Magn Reson Imaging 1992;10:497–511. https://doi.org/10.1016/0730-725X(92)90001-G.

[28] Ben-Eliezer N, Sodickson DK, Shepherd T, Wiggins GC, Block KT. Accelerated and motion-robust in vivo T_2 mapping from radially undersampled data using bloch-simulation-based iterative reconstruction. Magn Reson Med 2016;75:1346–54. https://doi.org/10.1002/mrm.25558.

[29] Schmitt P, Griswold MA, Jakob PM, Kotas M, Gulani V, Flentje M, et al. Inversion recovery TrueFISP: quantification of T_1, T_2, and spin density. Magn Reson Med 2004;51:661–7. https://doi.org/10.1002/mrm.20058.

[30] Deoni SCL, Rutt BK, Peters TM. Rapid combined T_1 and T_2 mapping using gradient recalled acquisition in the steady state. Magn Reson Med 2003;49:515–26. https://doi.org/10.1002/mrm.10407.

[31] Deoni SCL, Peters TM, Rutt BK. High-resolution T_1 and T_2 mapping of the brain in a clinically acceptable time with DESPOT1 and DESPOT2. Magn Reson Med 2005;53:237–41. https://doi.org/10.1002/mrm.20314.

[32] Poon CS, Henkelman RM. Practical T_2 quantitation for clinical applications. J Magn Reson Imaging 1992;2:541–53.

[33] Deoni SCL. Transverse relaxation time (T_2) mapping in the brain with off-resonance correction using phase- cycled steady-state free precession imaging. J Magn Reson Imaging 2009;30:411–7. https://doi.org/10.1002/jmri.21849.

[34] Sled JG, Pike GB. Correction for B_1 and B_0 variations in quantitative T_2 measurements using MRI. Magn Reson Med 2000;43:589–93.

[35] Hennig J. Multiecho imaging sequences with low refocusing flip angles. J Magn Reson 1988;78:397–407. https://doi.org/10.1016/0022-2364(88)90128-X.

[36] Hennig J. Echoes—how to generate, recognize, use or avoid them in MR-imaging sequences. Part I: fundamental and not so fundamental properties of spin echoes. Concepts Magn Reson 1991;3:125–43. https://doi.org/10.1002/cmr.1820030302.

[37] Ma D, Gulani V, Seiberlich N, Liu K, Sunshine JL, Duerk JL, et al. Magnetic resonance fingerprinting. Nature 2013;495:187–92. https://doi.org/10.1038/nature11971.

[38] Radunsky D, Barazany D, Ben Eliezer N. Analysis of magnetization transfer (MT) influence on quantitative mapping of T2 relaxation time. Magn Reson Med 2019;82:145–58. https://doi.org/10.1002/mrm.27704.

[39] Zhang X, Zhou Z, Chen S, Chen S, Li R, Hu X. MR fingerprinting reconstruction with Kalman filter. Magn Reson Imaging 2017;41:53–62. https://doi.org/10.1016/j.mri.2017.04.004.

[40] Nataraj G, Nielsen J, Scott C, Fessler JA. Dictionary-free MRI PERK: parameter estimation via regression with kernels. IEEE Trans Med Imaging 2018;37:2103–14. https://doi.org/10.1109/TMI.2018.2817547.Dictionary-Free.

[41] Cohen O, Zhu B, Rosen MS. MR fingerprinting Deep RecOnstruction NEtwork (DRONE). Magn Reson Med 2018;80:885–94. https://doi.org/10.1002/mrm.27198.

[42] Fang Z, Chen Y, Nie D, Lin W, Shen D. RCA-U-net: residual channel attention U-net for fast tissue quantification in magnetic resonance fingerprinting. Med Image Comput Comput Interv MICCAI. Int Conf Med Image Comput Comput Interv 2019;11766:101–9. https://doi.org/10.1007/978-3-030-32248-9_12.

[43] Liu F. Improving quantitative magnetic resonance imaging using deep learning. Semin Musculoskelet Radiol 2020;24:451–9. https://doi.org/10.1055/s-0040-1709482.

[44] Fang Z, Chen Y, Hung S-C, Zhang X, Lin W, Shen D. Submillimeter MR fingerprinting using deep learning-based tissue quantification. Magn Reson Med 2020;84:579–91. https://doi.org/10.1002/mrm.28136.

[45] Tao Q, Lelieveldt BPF, van der Geest RJ. Deep learning for quantitative cardiac MRI. AJR Am J Roentgenol 2020;214:529–35. https://doi.org/10.2214/AJR.19.21927.

[46] McGivney DF, Pierre E, Ma D, Jiang Y, Saybasili H, Gulani V, et al. SVD compression for magnetic resonance fingerprinting in the time domain. IEEE Trans Med Imaging 2014;33:2311–22. https://doi.org/10.1109/TMI.2014.2337321.

[47] Bipin Mehta B, Coppo S, Frances McGivney D, Ian Hamilton J, Chen Y, Jiang Y, et al. Magnetic resonance fingerprinting: a technical review. Magn Reson Med 2019;81:25–46. https://doi.org/10.1002/mrm.27403.

[48] Smith DS, Li X, Abramson RG, Quarles CC, Yankeelov TE, Welch EB. Potential of compressed sensing in quantitative MR imaging of cancer. Cancer Imaging 2013;13:633–44. https://doi.org/10.1102/1470-7330.2013.0041.

[49] Lustig M, Donoho D, Pauly JM. Sparse MRI: the application of compressed sensing for rapid MR imaging. Magn Reson Med 2007;58:1182–95. https://doi.org/10.1002/mrm.21391.

[50] Cauley SF, Setsompop K, Ma D, Jiang Y, Ye H, Adalsteinsson E, et al. Fast group matching for MR fingerprinting reconstruction. Magn Reson Med 2015;74:523–8. https://doi.org/10.1002/mrm.25439.

[51] Wang D, Ostenson J, Smith DS. snapMRF: GPU-accelerated magnetic resonance fingerprinting dictionary generation and matching using extended phase graphs. Magn Reson Imaging 2020;66:248–56. https://doi.org/10.1016/j.mri.2019.11.015.

[52] Jolliffe IT. Principal Component Analysis. 2nd ed. New York: Springer-Verlag; 2002. https://doi.org/10.1007/b98835.

[53] Hotelling H. Analysis of a complex of statistical variables into principal components. J Educ Psychol 1933;24:417–41. https://doi.org/10.1037/h0071325.

[54] Sirovich L. Low-dimensional procedure for the characterization of human faces. J Opt Soc Am A 2014;4:519–24. https://doi.org/10.1364/JOSAA.4.000519.
[55] Popiel T, Noakes L. Bézier curves and C 2 interpolation in Riemannian manifolds. J Approx Theory 2007;148:111–27. https://doi.org/10.1016/j.jat.2007.03.002.
[56] Radunsky D, Stern N, Nassar J, Tsarfaty G, Blumenfeld Katzir T, Ben Eliezer N. Quantitative platform for accurate and reproducible assessment of transverse (T2) relaxation time. NMR Biomed 2021. https://doi.org/10.1002/nbm.4537.